European Journal of Cell Biology 104 (2025) 151500

Contents lists available at ScienceDirect

European Journal of Cell Biology

journal homepage: www.elsevier.com/locate/ejcb

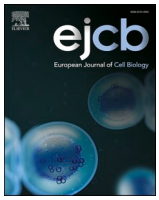

Genetic compensation highlights the importance of neural cell adhesion molecule Ncam1 paralogs in balancing signaling pathways during zebrafish lateral line development

Annemarie Lange, Martin Bastmeyer, Joachim Bentrop *

Karlsruhe Institute of Technology (KIT), Zoological Institute, Cell- and Neurobiology, Fritz-Haber-Weg 4, Karlsruhe 76131, Germany

ARTICLE INFO

Keywords:
Ncam1
Proliferation
FGF/Wnt signaling
Genetic compensation
Zebrafish
Lateral line system
Developmental biology

ABSTRACT

The neural cell adhesion molecule NCAM1 is essential for neuronal development and enables organized cell migration, axon growth, and fasciculation. As a result of genome duplication in zebrafish, the paralogs Ncam1a and Ncam1b arose. Our previously published findings using morpholino knockdown experiments demonstrated the essential role of Ncam1b in the development of the zebrafish lateral line system, a mechanosensory organ critical for detecting water movements. *ncam1b* morphants exhibited severe defects, including impaired primordium migration, disrupted proneuromast deposition, and reduced cell proliferation within the primordium. These defects were linked to a disrupted interaction between Ncam1b and Fgfr1a, which led to compromised proliferation and abnormal lateral line development. The current study reveals that *ncam1b* mutants, however, unlike morphants, do not show this severe phenotype. Instead, we observed subtle alterations, including altered FGF and Wnt signaling and a redistribution of proliferating cells within the primordium. Notably, *ncam1b* mutants displayed elevated levels of the paralog *ncam1a* mRNA. The knockdown of either *ncam1a* or *upf3a* in *ncam1b* mutants resulted in a phenotype resembling that of *ncam1b* morphants. Upf3a is a key regulator of genetic compensation, a well-known phenomenon in zebrafish research. This supports the hypothesis that upregulated *ncam1a* compensates for the loss of *ncam1b*, facilitating normal lateral line development. These findings emphasize the essential role of Ncam1 in zebrafish lateral line development and suggest that the retention of both paralogs, *ncam1a* and *ncam1b*, acts as a protective mechanism to ensure the preservation of critical Ncam1 functions after gene duplication.

1. Introduction

The posterior lateral line system (pLLS) of zebrafish is responsible for detecting water movements in the fish's environment (Dykgraaf, 1933). Due to its unique characteristics, it provides detailed insights into complex processes such as collective cell migration and axonal growth during the development of sensory organs (Aman and Piotrowski, 2008; Dambly-Chaudière et al., 2007; Gilmour et al., 2002; Kimmel et al., 1995; Lush and Piotrowski, 2014; Metcalfe et al., 1985). The pLLS originates from a primary sensory lateral line placode, which separates around 18 h post-fertilization (hpf) into the posterior lateral line ganglion (pLLG) and the posterior primary primordium (primI) (Ghysen and Dambly-Chaudière, 2007; Kimmel et al., 1995; Metcalfe et al., 1985). PrimI consists of approximately 100 cells that migrate caudally along the horizontal myoseptum, reaching the tip of the tail by about 40–48 hpf (Kimmel et al., 1995; Metcalfe et al., 1985). During this migration, primI periodically deposits primary proneuromasts, which then differentiate into neuromasts, the organs containing the sensory hair cells (Ghysen and Dambly-Chaudière, 2007). PrimI exhibits distinct anterior-posterior polarity characterized by morphological and signaling differences between its leading part (Leading Zone) and trailing part (Trailing Zone). In the Leading Zone, Wnt signaling triggers *lef1* expression, stimulating the proliferation of primordial pseudomesenchymal cells (Gamba et al., 2010; Lecaudey et al., 2008). Conversely, in the Trailing Zone, Fgfr1a-dependent signaling activates *erm*, promoting epithelial cell proliferation (Aman and Piotrowski, 2008; Lecaudey et al., 2008). Additionally, FGF signaling orchestrates rosette formation, leading to the deposition and development of sensory neuromasts (Aman and Piotrowski, 2008; Lecaudey et al., 2008). Our lab previously demonstrated that the Neural Cell Adhesion Molecule 1

* Corresponding author.
E-mail address: joachim.bentrop@kit.edu (J. Bentrop).

https://doi.org/10.1016/j.ejcb.2025.151500
Received 21 March 2025; Received in revised form 18 June 2025; Accepted 18 June 2025
Available online 19 June 2025

(Ncam1) is expressed in the zebrafish pLLS (Langhauser et al., 2012). NCAM1, in general, is a well-characterized glycoprotein of the immunoglobulin superfamily which plays crucial roles in regulating cell adhesion, proliferation, migration, neurogenesis and neuronal plasticity (Hinsby et al., 2004). Its protein structure, comprising five immunoglobulin-like (Ig) domains and two fibronectin (FN) domains, enables various homophilic and heterophilic interactions (Cunningham et al., 1987). Due to a genome duplication, zebrafish possess two *ncam1* paralogs: *ncam1a* and *ncam1b*. In embryonic development, these paralogs have subfunctionalized roles, as we have previously shown for the formation of the posterior commissure and for outgrowth, fasciculation and pathfinding of spinal motor axon bundles (Langhauser et al., 2012). *ncam1a* and *ncam1b* are also expressed in various structures of the pLLS, including the ganglion (pLLG), nerve (pLLN), neuromasts and primI (Dries et al., 2021). Here, their subfunctionalization is further evidenced by the distinct phenotypes following morpholino-mediated knockdown (Dries et al., 2021). A knockdown of *ncam1a* affects pLLS development by reducing both the migration distance of primI and the number of deposited proneuromasts. In contrast, the knockdown of *ncam1b* results in a more severe phenotype characterized by significantly slowed and partially misdirected migration of a smaller primI. In addition, formation and deposition of proneuromasts are rarely observed. We attributed this severe *ncam1b* knockdown phenotype to a lack of heterophilic interactions between Ncam1b and Fgfr1a in the Trailing Zone, leading to reduced FGF signaling, decreased *erm* expression and less proliferation (Dries et al., 2021). Furthermore, homophilic binding of Ncam1b between neighboring cells might play a crucial role in stabilizing newly formed proneuromasts. Consequently, the absence of Ncam1b leads to the disintegration of proneuromasts. To further validate and expand upon these findings, we considered it crucial to conduct additional investigations using CRISPR/Cas9 induced *ncam1b* mutants.

Genetic compensation is a fascinating biological process that explains the genetic robustness observed in organisms, allowing them to maintain fitness despite genetic disruptions (Rossi et al., 2015). This phenomenon has been extensively studied in various model organisms, particularly in zebrafish, where mutants often fail to exhibit the severe phenotypes observed in morphants for the same genes (Kettleborough et al., 2013). Recent research has shed light on the mechanisms underlying genetic compensation, revealing a complex interplay of molecular processes. The genetic compensation response (GCR) is triggered by the upregulation of compensating genes through nonsense-mediated decay (NMD), which recognizes and degrades mRNAs containing premature stop codons (PMSCs) to prevent the translation of faulty proteins (El-Brolosy et al., 2019). In this process, the presence of a PMSC in mutant mRNAs, along with sequence homology between the mutant and compensatory genes, activates compensatory mechanisms. These responses are also regulated by epigenetic factors. While some studies suggest that Upf3a binding and Wdr5 recruitment lead to increased H3K4me3 methylation at compensatory genes (Ma et al., 2019), others indicate that genetic compensation can occur independently of these pathways (Xie et al., 2023). This implies that multiple mechanisms might be involved in activating compensatory genes in response to genetic mutations.

The current study reveals that Ncam1b plays an important role in spatially regulating cell proliferation within the primordium by maintaining the balance between the FGF and Wnt signaling. When *ncam1b* is absent, this balance is disrupted, leading to alterations in the distribution of proliferating cells. While *ncam1b* morphants exhibited significant defects in primordium migration, proneuromast deposition, and cell proliferation (Dries et al., 2021), *ncam1b* mutants show only subtle changes. This difference in phenotype between mutants and morphants is likely due to the upregulation of the paralog *ncam1a* in response to the knockout of *ncam1b*. The knockdown of either *ncam1a* or *upf3a*, a key regulator of genetic compensation, in *ncam1b* mutants reproduced the morphant phenotype, demonstrating that *ncam1a* compensates for the loss of *ncam1b*. These findings emphasize the functional importance of retaining both paralogs after gene duplication to ensure the proper execution of critical developmental processes.

2. Results

2.1. *ncam1b* mutants phenocopy wild type lateral line development, unlike the pronounced phenotype seen in *ncam1b* morphants

The zebrafish posterior lateral line primordium (primI) begins its migration around 24 hpf, following the horizontal myoseptum for the next 24 h until it reaches the tip of the tail. During migration, primI deposits 5–6 proneuromasts, each consisting of about 30 cells, that later differentiate into mature neuromasts. Cell adhesion, communication and proliferation play crucial roles during this collective and directional cell migration and proneuromast deposition. We have previously demonstrated the importance of the neural cell adhesion molecules Ncam1a and Ncam1b during this process (Dries et al., 2021). Morpholino (MO)-mediated knockdown of *ncam1b* results in a severe phenotype characterized by a strongly reduced migration distance of a smaller primI and fewer deposited neuromasts. *ncam1a* morphants exhibit a milder phenotype. Given the more pronounced phenotype observed in *ncam1b* morphants, we focused in the current study primarily on Ncam1b. To elucidate the specific role of *ncam1b* in lateral line development, we generated a homozygous *ncam1b* deletion (*n1b* -/- Del) mutant, deleting ca. 200,000 bp of the coding region and creating a stop codon 33 bp after the start codon (Supp. 1 A–A''). Additionally, a second mutant containing a premature stop codon in Exon1 was generated (*n1b* -/- PMSC), with a stop codon after 42 bp (Supp. 1 B). Both *ncam1b* mutants show no detectable Ncam1b protein in immunostaining experiments (Supp. 2 A–J). Furthermore, droplet digital PCR (ddPCR) analysis at 36 hpf revealed significantly reduced *ncam1b* mRNA levels in the *n1b* -/- PMSC, suggesting nonsense-mediated mRNA decay (Supp. 2 K green bar). In the *n1b* -/- Del mutant, ddPCR analysis demonstrated that the targeted region was also undetectable at the mRNA level, confirming the effectiveness of the deletion (Supp. 2 K red bar).

In this study we were able to reproduce the severe phenotype of *ncam1b* morphants (Fig. 1 B, E–G). In contrast, *ncam1b* mutants show normal development of the pLLS (Fig. 1 C + D, E–G). At 48 hpf, primI in *ncam1b* mutants has successfully completed its migration (Fig. 1 E), reaching the tip of the tail, just like in wild type embryos. PrimI in *ncam1b* mutants is of normal size, showing no apparent differences from wild type primordia (Fig. 1 F). Furthermore, during its migration along the horizontal myoseptum, primI in *ncam1b* mutants deposited the expected number of 6 proneuromasts (Fig. 1 G). The normal timing of migration, primI size, and proneuromast deposition suggest that the knockout of *ncam1b* does not significantly impact collective cell migration or the ability of primI to form and deposit proneuromasts. This striking contrast between the severe phenotype observed in *ncam1b* morphants and the normal development seen in *ncam1b* knockout mutants raises crucial questions about the underlying causes.

2.2. Subtle phenotypic changes in signaling and proliferation in *ncam1b* mutant lateral line primordium

Dries et al. (2021) reported significant alterations in primI development in *ncam1b* morphants, including disruptions in Wnt and FGF signaling. Using color *in situ* hybridization, they observed expanded expression of the Wnt-target gene *lef1* in the Leading Zone and reduced expression of the FGF target gene *erm* in the Trailing Zone, despite normal *fgfr1a* receptor expression. In our current study, we successfully reproduced the *ncam1b* morphant phenotype using fluorescence *in situ* hybridization (FISH) (Fig. 2 A''–B'', A'''–B''', D–F). We then extended the investigation to include *ncam1b* mutants, revealing similar, albeit less pronounced, alterations in Wnt and FGF signaling. Specifically, we observed reduced expression of the FGF target gene *erm* and expanded expression of the Wnt target gene *lef1* (Fig. 2 C''–C''', D–F), despite

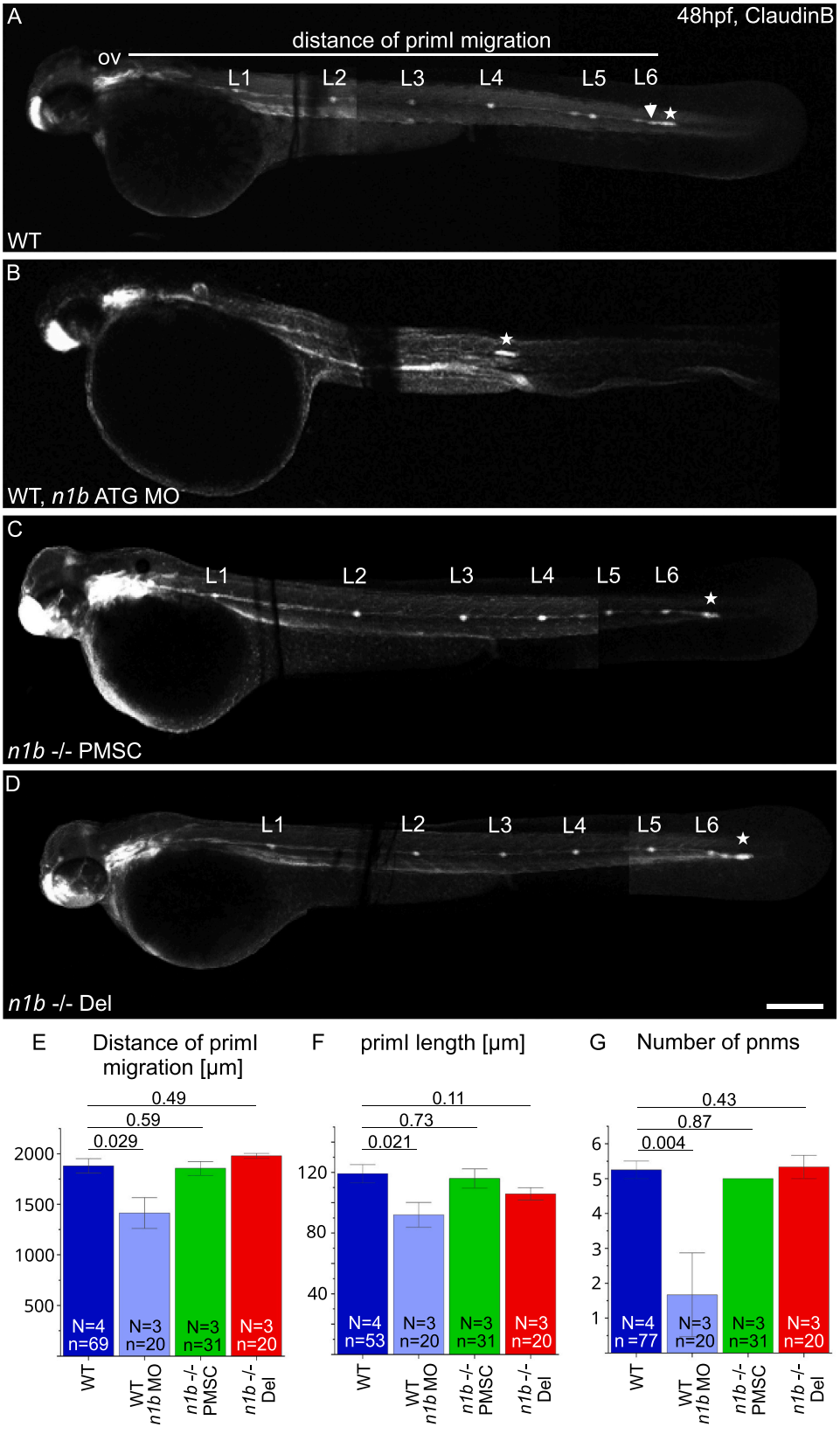

(caption on next page)

Fig. 1. *ncam1b* knockdown and knockout leads to different phenotypes in the development of the lateral line system. (A–D) Lateral views of 48 hpf *Tg(ClaudinB::lynGFP)* (A) Wild type (WT) (B) *n1b* morphant, (C) *n1b* -/- PMSC and (D) *n1b* -/- Del. Embryos are oriented with rostral to the left and dorsal to the top. (A) At 48 hpf, primI (star) of WT reaches the tip of the tail and deposits 6 proneuromasts (L1-L6), with the last one having just been deposited (arrow). The migration distance was measured from the otic vesicle (ov) to primI. (B) *ncam1b* morpholino injection leads to reduced migration of a smaller primI and deposition of fewer proneuromasts. (C + D) *n1b* -/- PMSC and *n1b* -/- Del mutants phenocopy the WT phenotype, with primI reaching the tip of the tail at 48 hpt and depositing 6 proneuromasts (L1-L6). (E–G) Quantification of migration distance, primI length and number of proneuromasts in WT, *ncam1b* morpholino injected embryos, *n1b* -/- PMSC and *n1b* -/- Del. Bars indicate mean values of the medians of each experiment, with error bars representing standard error. Statistic was made using two-sided *t*-test. Scale bar 200 μm. *Abbreviations: WT: Wild type; n1b -/- PMSC: ncam1b -/- Premature Stop Codon mutant; n1b -/- Del: ncam1b deletion mutant; MO: Morpholino; primI: primordium; pnm: proneuromast; ov: otic vesicle.*

unchanged levels of *fgfr1a* receptor expression (Fig. 2 E + Supp. 3). The milder effects observed in mutants suggest potential compensatory mechanisms that may be activated in genetic knockouts but not in morpholino-mediated knockdowns.

We have previously found that *ncam1b* morphants exhibit reduced cell proliferation in primI, alongside decreased *erm* expression (Dries et al., 2021). This is thought to result from the interaction of Ncam1b with Fgfr1a in the Trailing Zone. In the current study, in contrast, we find no statistically significant difference in the total number of BrdU positive (BrdU+) cells between WT and *ncam1b* mutant embryos (Fig. 2 G–H, I). To investigate potential spatial differences, we performed a morphological segmentation of primI into Leading and Trailing Zones (Fig. 2 J). While total primI length remained comparable between WT and *ncam1b* mutants (Supp. 4 A), we find a significant expansion of the Leading Zone in mutants (Fig. 2 K). Based on the morphological segmentation of zones, we observed a distinctly different distribution of BrdU+ cells (Fig. 2 L). In wild type embryos, a substantial majority of the BrdU+ cells were found in the Trailing Zone. The Trailing Zone of *ncam1b* mutants, in contrast, contained a significantly lower percentage of proliferating cells. In comparison, the Leading Zone of wild type primI contained only half as many BrdU+ cells as the Leading Zone in *ncam1b* mutants. To quantify this shift, we measured proliferation density in the Leading and Trailing Zones (Fig. 2 M). Proliferation density was significantly higher in the Leading Zone of *ncam1b* mutants than in wild type, while no significant difference was observed in the Trailing Zone (Fig. 2 M). This indicates that increased proliferative activity in *ncam1b* mutants is specific to the expanded Leading Zone, highlighting a functional shift associated with altered Wnt/FGF signaling and disrupted zonation.

2.3. Ncam1a is upregulated in ncam1b mutants

The discrepancy between severe morphant and mild mutant phenotypes led us to speculate that genetic compensation could be involved. Genetic compensation is a phenomenon in which the upregulation of related genes compensates for the loss of the gene of interest in mutants, thereby masking the morphant phenotype (Rossi et al., 2015). The zebrafish possess a paralog of *ncam1b*, namely *ncam1a*, due to a genome duplication event in the teleost lineage (Vandepoele et al., 2004). *ncam1a* shares 66 % homology with *ncam1b* (Mizuno et al., 2001).

Using ddPCR, we found that *ncam1a* mRNA levels were significantly upregulated in *ncam1b* mutant embryos, whereas no such upregulation was observed in *ncam1b* morphants (Fig. 3 A). In addition, immunostaining shows increased Ncam1a expression in the primI of *ncam1b* mutants (Fig. 3 B–D). Together these results suggest that loss of *ncam1b* triggers compensatory upregulation of *ncam1a*. This response may explain the milder mutant phenotype and underscores the complexity of gene function and regulation during development.

2.4. Knockdown of either upf3a or ncam1a in ncam1b mutants partially phenocopies the ncam1b-knockdown phenotype

To analyze a potential role of genetic compensation in the upregulation of *ncam1a* in *ncam1b* mutants, we examined the effects of knocking down *upf3a*, a key regulator of genetic compensation, and *ncam1a* in *ncam1b* mutants. Upf3a plays a crucial role in the homology dependent genetic compensation response (HDGCR) by interacting with mRNAs containing a premature stop codon and activating transcription factors that upregulate homologous genes proteins (Lykke-Andersen and Jensen, 2015, El-Brolosy et al., 2019). To enhance clarity, the results for *upf3a* (Fig. 4) and *ncam1a* (Fig. 5) are presented in two figures, with datasets from wild type, deletion mutants, and *ncam1b* morphants being consistent across both figures. All statistical analyses for these experiments were performed using ANOVA with Scheffé post hoc test to minimize the risk of false positive results due to multiple comparisons. We find a striking contrast in the effects of the *upf3a* knockdown between wild type and *ncam1b* mutant zebrafish. While injection of the *upf3a* MO into wild type embryos did not significantly alter pLLS development (Fig. 4 D, F–H), the same knockdown in *ncam1b* mutants led to a phenotype closely resembling that of *ncam1b* morphants (Fig. 4 E–H). Notably, pLLS development in *upf3a* MO injected *ncam1b* mutants differed significantly from uninjected *ncam1b* mutants. The latter show normal development of the pLLS (Fig. 4 B). This suggests that *upf3a* plays a key role in mediating a compensatory response in *ncam1b* mutants, counterbalancing the deficiency of *ncam1b*. In contrast, injection of the *upf3a* MO into wild type zebrafish did not result in significant differences in the development of the pLLS (Fig. 4 D, F–H).

Next, we investigated whether the upregulated paralog *ncam1a* plays a complementary role in alleviating the impact of the *ncam1b* deficiency (Fig. 5). We injected a *ncam1a* MO into wild type (Fig. 5 D, F–H) and *ncam1b* mutant embryos (Fig. 5 E, F–H). In our study, ANOVA with Scheffé post hoc test did not reveal significant differences in pLLS development or primI size after *ncam1a* knockdown (Fig. 5 D, F–H). This contrasts with the findings of Dries et al. (2021), who reported a mild phenotype using a *t*-test. The discrepancy may be due to the more stringent statistical correction applied in our analysis, which reduces the likelihood of false positives when comparing multiple groups. In contrast, a *ncam1a* knockdown in *ncam1b* mutants resulted in a severe phenotype similar to that of the *ncam1b* morpholino knockdowns (Fig. 5 E–H). This substantiates our hypothesis that Ncam1a has a compensatory function for the loss of Ncam1b, particularly in pLLS development.

In summary, our findings suggest that *upf3a* mediates genetic compensation in zebrafish *ncam1b* mutants. *ncam1a* acts as the compensator in that response.

3. Discussion

3.1. Discrepancies between ncam1b morphant and mutant phenotype

This study investigates neural cell adhesion molecule 1b (Ncam1b) in zebrafish posterior lateral line system (pLLS) development. While *ncam1b* morphants have severe pLLS development defects (reduced primordium (primI) migration, fewer deposition of proneuromasts) (Fig. 1, see also Dries et al. 2021), CRISPR-Cas9-induced *ncam1b* mutants exhibit normal pLLS development with only subtle molecular changes. Such morphant-mutant discrepancies are well-documented in zebrafish research, as ~ 80 % of morpholino phenotypes lack knockout model replication (Kettleborough et al., 2013). While off-target effects of the *ncam1b*-morpholino are unlikely (Langhauser et al. 2012; Dries et al. 2021) genetic compensation in mutants and differences between acute and chronic loss-of-function effects may explain these differences, consistent with findings in other mutants (El-Brolosy et al., 2019; Kok

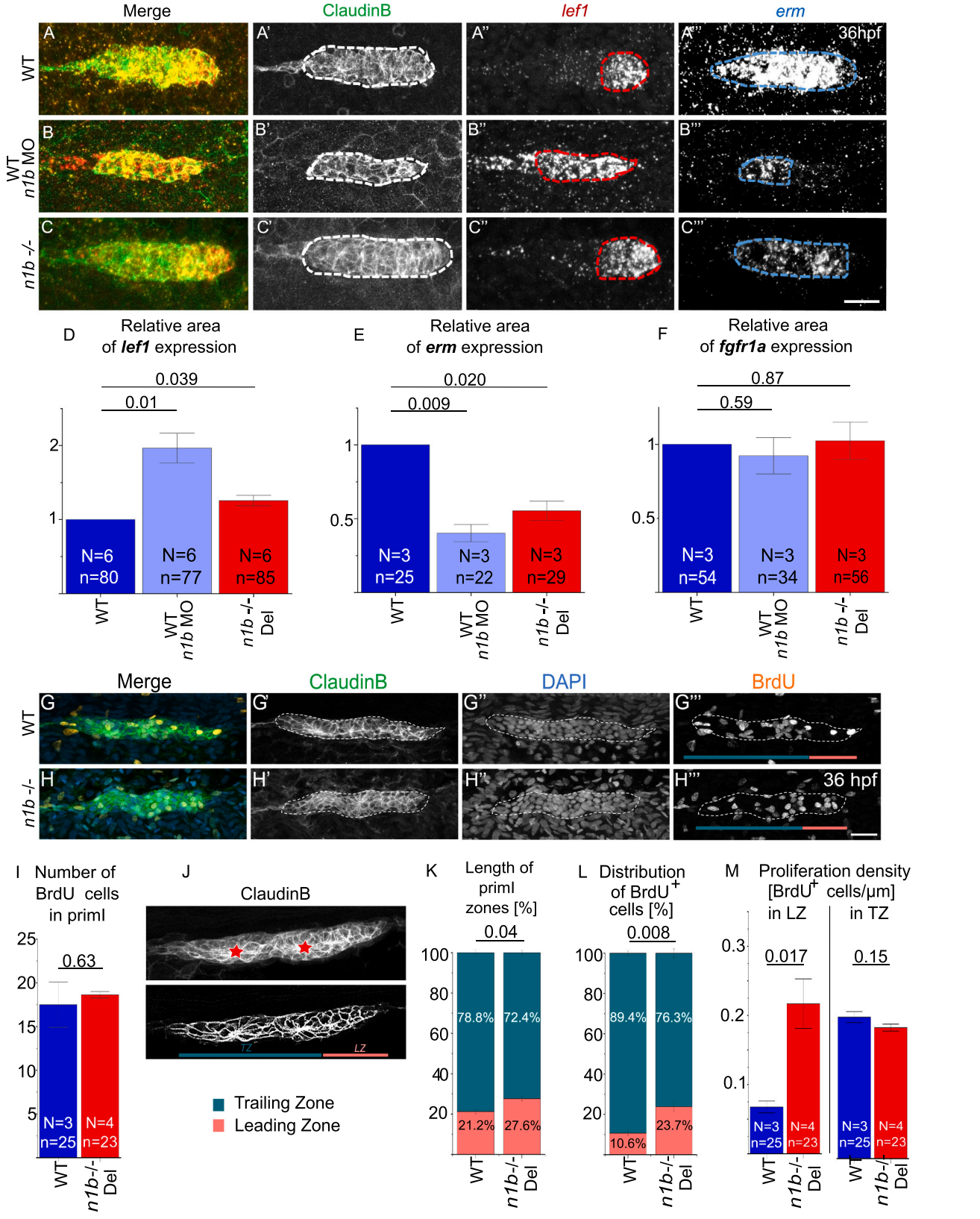

(caption on next page)

Fig. 2. Loss of *ncam1b* leads to small differences in signaling and proliferation within the migrating primordium. (A-C) Fluorescence *in situ* hybridization of 36 hpf *Tg (ClaudinB::lynGFP)* primordia in (A) WT, (B) *ncam1b* morphants, and (C) *n1b -/-* Del. Areas for expression analysis were delineated in Fiji by drawing around regions that displayed a strong signal compared to the background, while regions with only weak or faint signals were excluded. Red outline indicates *lef1* expression area, blue outline indicates *erm* expression area. (D–F) Quantification of regions expressing (D) *lef1*, (E) *fgfr1a* (microscopy images shown in Supp. 3), and (F) *erm*. *ncam1b* absence leads to an enlarged *lef1* region and a reduced *erm* region, *fgfr1a* expression domain is unaffected. (G–M) BrdU staining reveals changes in proliferating cell distribution. (G-H) WT and *ncam1b* mutant *Tg(ClaudinB::lynGFP)* embryos were treated with BrdU at 36 hpf for 20 min and immunostained for BrdU (orange), GFP (green) and DAPI (blue) as indicated. Color bars in (G''' + H''') indicate the respective zones in turquoise for the Trailing Zone and reddish for the Leading Zone. (I) Numbers of BrdU-positive cells in WT and *n1b -/-* Del primordia. (J) Illustration of the subdivision of primI into Leading (LZ) and Trailing Zones (TZ) based on cell morphology. The upper panel shows the original image, while in the lower panel the contrast was enhanced to better visualize morphological differences between the TZ and LZ. Cells in the TZ are organized into rosette-like proneuromasts (epithelial character). They are arranged radially around a central prospective first hair cell (asterisk). The cells in the LZ display a more randomly oriented, mesenchymal-like morphology. (K) Changes in the length of Leading and Trailing Zone in *ncam1b* mutants compared to the wild type. (L) Redistribution of proliferating cells within Leading and Trailing Zones. (M) Proliferation density, as calculated by dividing the number of BrdU+ cell by the zone length, is significantly higher in the Leading Zone of *ncam1b* mutants compared to wild type. Bars indicate mean values of the medians of each experiment, with error bars representing standard error. Statistical test for (D–F, I, M): Two-sided *t*-test and for (K+L): χ^2-test. Scale bars 20 μm. *Abbreviations: WT: Wild type; n1b -/- Del: ncam1b deletion mutant; MO: Morpholino; primI: primordium; TZ: Trailing Zone; LZ: Leading Zone.*

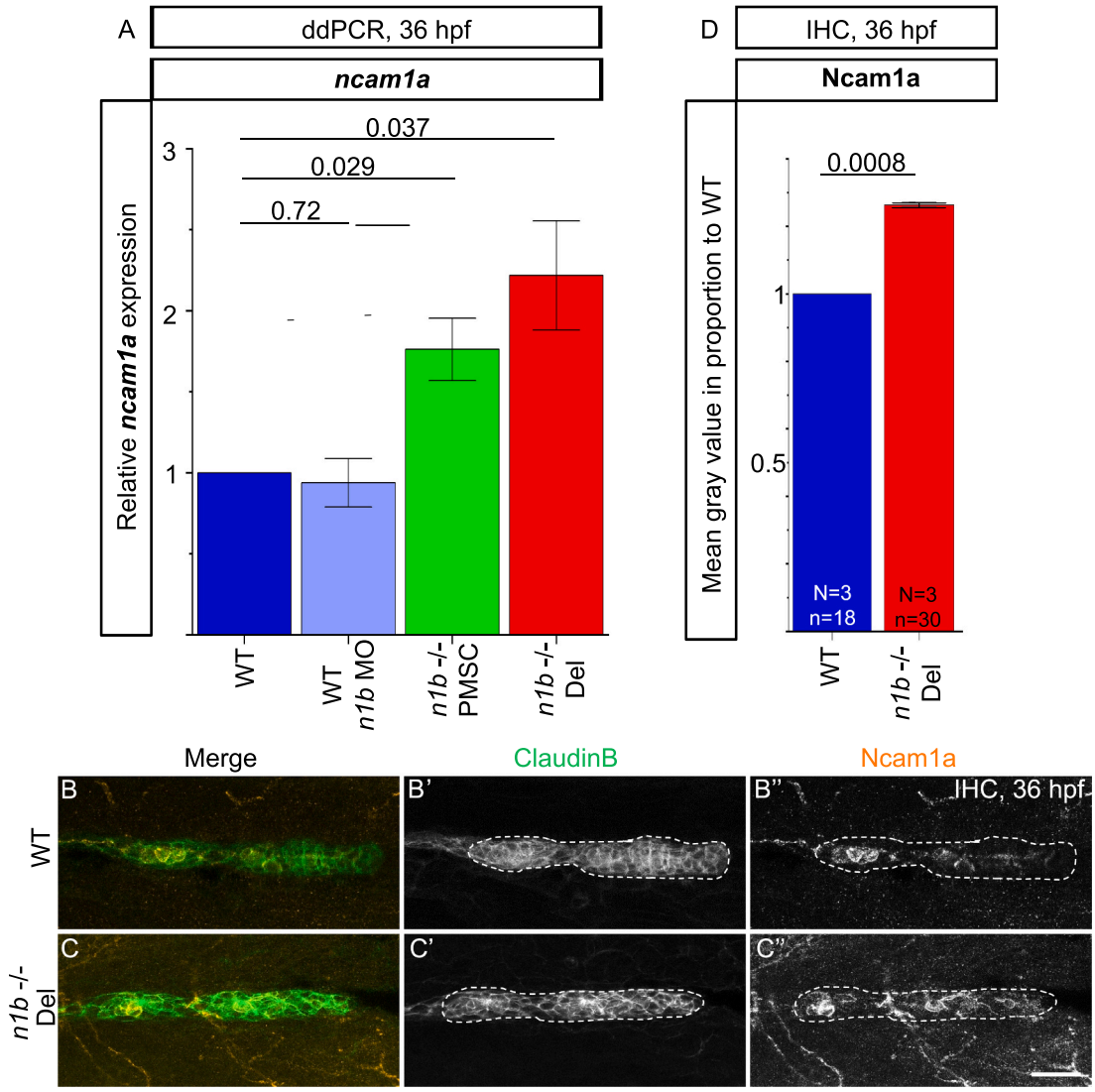

Fig. 3. Upregulation of *ncam1a* in *ncam1b* mutant embryos. (A) ddPCR measurements normalized to the housekeeping gene *β*-actin show significant upregulation of *ncam1a* and in *ncam1b* mutants, but not in *ncam1b* morphants, at 36 hpf. Mean gene expression levels were determined using biological triplicates or quadruplicates, each representing the mean of technical duplicates. Wild type (WT), *n1b -/-* PMSC mutants, and *n1b -/-* Del mutants were analyzed, with pools of 100 embryos per condition. (B–D) Ncam1a expression (orange) in the migrating primordium (primI). (B) *Tg(ClaudinB::lynGFP)*, serving as wild type, and (C) *ncam1b -/-* Del*; Tg (ClaudinB::lynGFP)*. (B' + C') Utilizing *ClaudinB::lynGFP* expression, a threshold was set to delineate the outline of primI (white border), Ncam1a expression in this region (B'' + C'') was quantified by mean grey value measurement of using Fiji. (D) The mean grey value of the *n1b -/-* Del mutant normalized to the WT shows a significant upregulation of Ncam1a expression. Statistic was made using one sample *t*-test. Scale bar 20 μm. *Abbreviations: WT: Wild type; n1b -/- PMSC: ncam1b -/- Premature Stop Codon mutant; n1b -/- Del: ncam1b deletion mutant; IHC: Immunohistochemistry*.

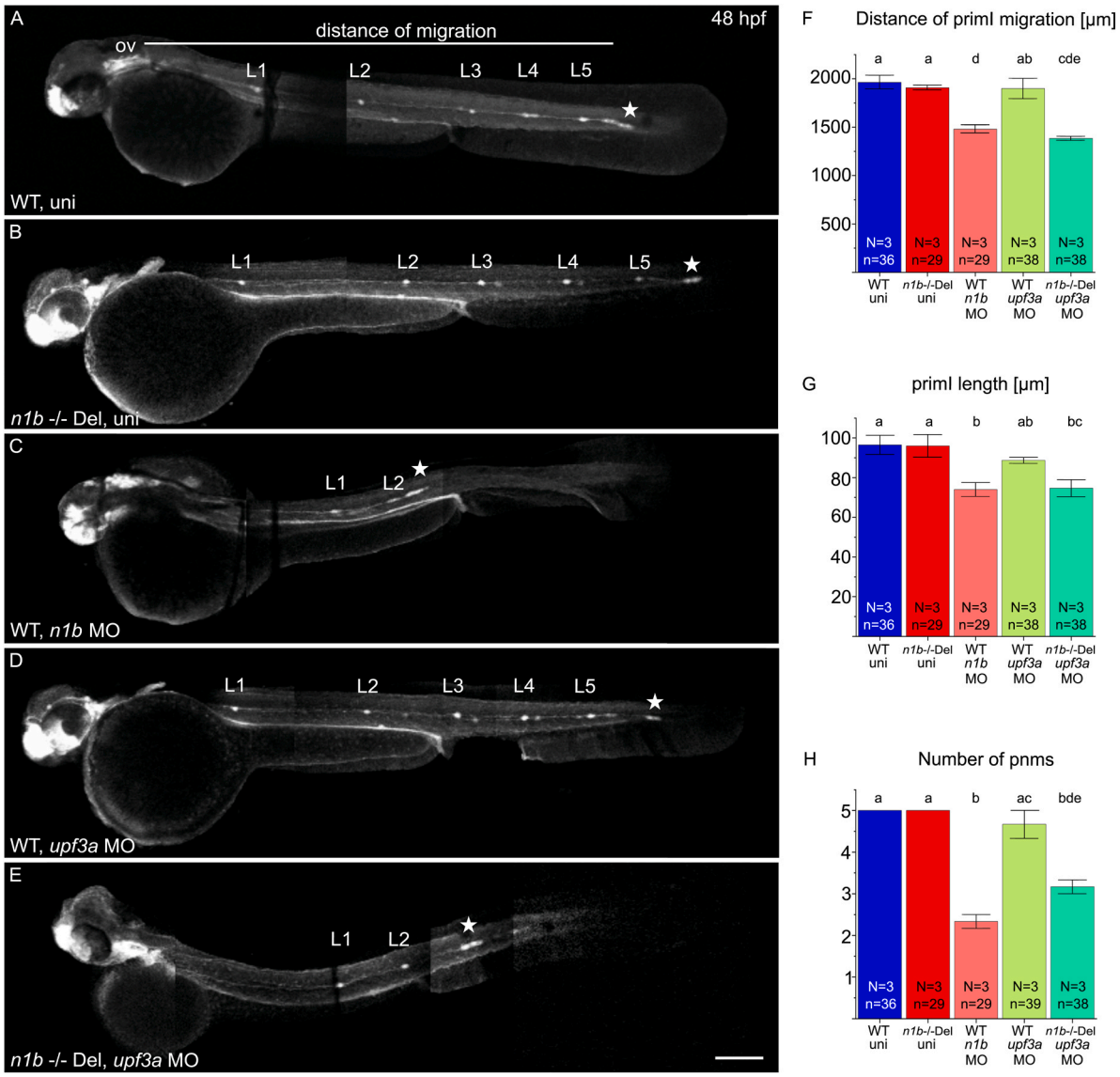

Fig. 4. Knockdown of *upf3a* in *ncam1b* mutants partially phenocopies the *ncam1b* knockdown phenotype. (A–E) Lateral views of 48 hpf *Tg(ClaudinB::lynGFP)* (A) Wild type uninjected (WT uni) (B) *n1b -/-* Del uninjected, (C) *n1b* MO in WT, (D) *upf3a* MO in WT and (E) *upf3a* MO in *n1b -/-* Del. Embryos are oriented with rostral to the left and dorsal to the top. (A) At 48 hpf, primI (star) of WT reaches the tip of the tail and deposits 5 proneuromasts (L1–L5). The migration distance was measured from the otic vesicle (ov) to primI. (B) *n1b -/-* Del mutants show the same phenotype as WT, with primI reaching the tip of the tail and 5 deposited proneuromasts. (C) *ncam1b* MO injection leads to reduced migration of a smaller primI and deposition of fewer proneuromasts. (D) *upf3a* MO injection in WT does not induce any defects in lateral line system development. (E) *upf3a* MO injection in *n1b -/-* Del leads to reduced primI migration and fewer deposited neuromasts. (F–H) Quantification of migration distance, primI length and number of proneuromasts. Bars indicate mean values of relative numbers, with error bars representing standard error. Differences between the five groups were analyzed using a one-way ANOVA followed by Scheffé post hoc tests. Differences were considered significant if the F-value exceeded the critical Scheffé value ($p < 0.05$). Groups that share the same letter do not differ significantly. Groups with different letters show significant differences in their means. Scale bar 200 µm. *Abbreviations: WT: Wild type; n1b -/- Del: ncam1b deletion mutant; MO: Morpholino; uni: uninjected; primI: primordium; pnm: proneuromast, ov: otic vesicle.*

et al., 2015; Rossi et al., 2015; Zhu et al., 2017).

3.2. Changes in signaling and proliferation in ncam1b mutants

Our results confirm the *ncam1b* morphant phenotype reported by Dries et al. (2021) but reveal key morphant/mutant differences in the zebrafish pLLS. Both exhibit enlarged *lef1*- and reduced *erm*-expressing regions in primI, with more pronounced effects in the morphants (Fig. 2 A–F). However, while morphants show reduced proliferation, as compared to the wild type, mutants only exhibit a redistribution of proliferating cells to the Leading Zone (Fig. 2 K–M). This correlates with *erm* decrease in the Trailing Zone and *lef1* increase in the Leading Zone. It suggests that Ncam1b fine-tunes FGF/Wnt pathways to regulate proliferation.

Proliferating cell redistribution in mutant primordia suggests that *lef1*-induced proliferation in the Leading Zone compensates for reduced Trailing Zone proliferation caused by downregulation of *erm*. In the morphants, however, *lef1* upregulation alone cannot drive proliferation, implying that additional factors are required, as proposed by McGraw et al. (2011). These factors are affected by the *ncam1b* MO knockdown but compensated for in the *ncam1b* mutant.

3.3. Role of upf3a-mediated genetic compensation by ncam1a in ncam1b mutants during lateral line development

The premature stop codon (PMSC) in *ncam1b* mutants (Supp. 1),

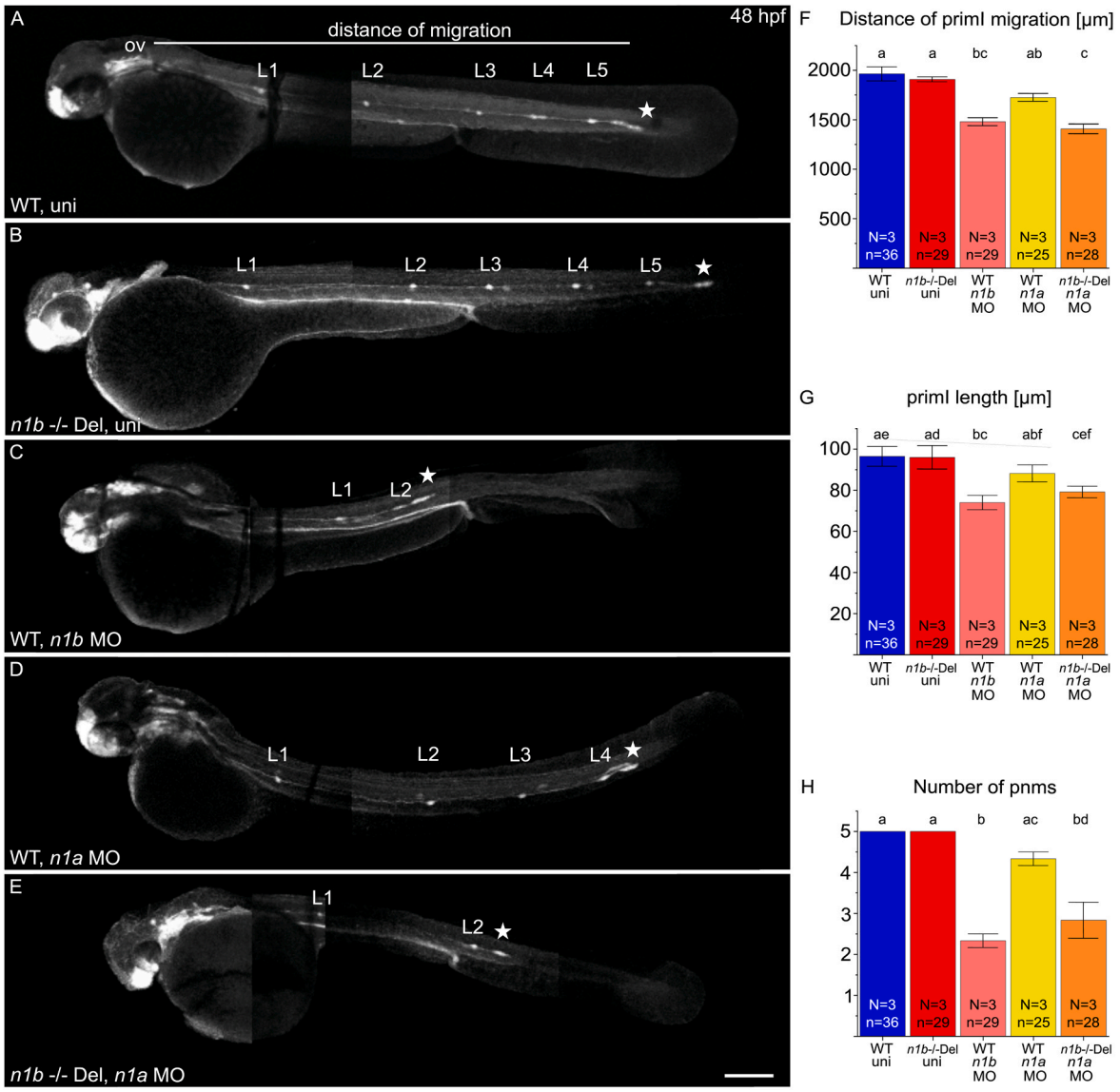

Fig. 5. Knockdown of *ncam1a* in *ncam1b* mutants phenocopies the *ncam1b* knockdown phenotype. (A–E) Lateral views of 48 hpf *Tg(ClaudinB::lynGFP)* (A) Wild type uninjected (WT uni) (B) *n1b* -/- Del uninjected, (C) *n1b* MO in WT, (D) *ncam1a* MO in WT and (E) *ncam1a* MO in *n1b* -/- Del. Embryos are oriented with rostral to the left and dorsal to the top. (A) At 48 hpf, primI (star) of WT reaches the tip of the tail and deposits 5 proneuromasts (L1–L5). The migration distance was measured from the otic vesicle (ov) to primI. (B) *n1b* -/- Del mutants show the same phenotype as WT, with primI reaching the tip of the tail and 5 deposited proneuromasts. (C) *ncam1b* MO injection leads to reduced migration of smaller primI and deposition of fewer proneuromasts. (D) Injection of the *ncam1a* MO in wild type zebrafish caused moderate defects in lateral line system development, but these effects did not reach statistical significance. (E) *ncam1a* MO injection in *n1b* -/- Del induce reduced migration of a smaller primI and fewer deposited neuromasts. (F-H) Quantification of migration distance, primI length and number of proneuromasts. Bars indicate mean values of the medians of each experiment, with error bars representing standard error. Differences between the five groups were analyzed using a one-way ANOVA followed by Scheffé post hoc tests. Differences were considered significant if the F-value exceeded the critical Scheffé value ($p < 0.05$). Groups that share the same letter do not differ significantly. Groups with different letters show significant differences in their means. Scale bar 200 µm. *Abbreviations: WT: Wild type; n1b -/- Del: ncam1b deletion mutant; MO: Morpholino; uni: uninjected; primI: primordium; pnm: proneuromast; ov: otic vesicle.*

likely activates the nonsense-mediated decay (NMD) pathway and triggers compensatory responses like the upregulation of homologous genes (El-Brolosy et al., 2019; Lykke-Andersen and Jensen, 2015). In line with this hypothesis, we observe an upregulation of *ncam1a* mRNA and Ncam1a protein in *ncam1b* mutant embryos (Fig. 3 A). Upregulated Ncam1a may partially compensate for Ncam1b loss by binding to Fgfr1a in the Trailing Zone and thereby restore the lost *erm* activity observed in the morphant (Dries et al., 2021).

Morpholino experiments support our hypothesis that *ncam1a* compensates for *ncam1b* loss in mutants. While knocking down *ncam1a* causes only mild pLLS defects in wild type embryos, which are not significant as judged by ANOVA analysis (Fig. 5, see also Dries et al. 2021), the same *ncam1a* knockdown leads to severe defects in *ncam1b* mutants.

A key factor driving the upregulation of homologous genes in the NMD pathway is Upf3a (Lykke-Andersen and Jensen, 2015; Shum et al., 2016; Yi et al., 2022). Its knockdown in *ncam1b* mutants recapitulates the *ncam1b* morphant phenotypes (Fig. 4) confirming its critical role in genetic compensation in the mutants. Milder than expected phenotypes, given that *ncam1b* mutants lacking *upf3a* would be deficient in both the *ncam1b* gene product and the *upf3a*-mediated genetic compensation response, suggest the existence of additional compensatory pathways. This highlights the complexity of genetic compensations network in zebrafish pLLS development.

3.4. Ncam1b regulates FGF and Wnt signaling pathways and proliferation in the migrating primordium

Our findings and conclusions can be summarized as follows (Fig. 6): (A) In wild type zebrafish, Ncam1b activates FGF signaling *via* interaction with Fgfr1a, inducing the expression of (i) *erm*, which promotes cell proliferation in the Trailing Zone, and of (ii) Wnt inhibitor *dkk*. In the Leading Zone, Wnt signaling drives proliferation *via* expression of *lef1* and inhibits FGF signaling *via* expression of *sef*. (B) In *ncam1b* morphants, reduced FGF signaling decreases *erm* expression and cell proliferation in the Trailing Zone (black flash) (Dries et al., 2021). Diminished Dkk1 allows Wnt/*lef1* expansion, but overall proliferation declines, suggesting the involvement of additional, yet unknown proliferative factors. (C) In *ncam1b* mutants, upregulated Ncam1a interacts with Fgfr1a, though less effectively than Ncam1b (Dries et al., 2021). Compared to wild type, FGF signaling is consequently reduced, though not as strong as in morphants. This causes a moderate decrease in *erm* expression and cell proliferation in the Trailing Zone. Simultaneously, Wnt signaling and consequent *lef1* expression expand in the Leading Zone. Thus, total proliferation remains stable, but its spatial distribution shifts.

In essence, Ncam1b is essential for maintaining the balance between FGF and Wnt signaling for spatial regulation of cell proliferation in the pLLS primordium. *ncam1b* loss disrupts this equilibrium, altering proliferating cell distribution, though overall proliferation persists *via* compensatory upregulation of *ncam1a*. The crucial role of *upf3a* in this process highlights the complexity of genetic compensation, where multiple genes and pathways collaborate to maintain normal development when key genes are lost.

4. Materials and methods

4.1. Fish strains and animal care

In our experiments, we used the transgenic fish strain *Tg(ClaudinB::lynGFP)*, which was kindly given to us by Darren Gilmour (University of Zurich, CH) (Haas and Gilmour, 2006). Zebrafish were maintained at 28.5 °C under standard conditions in a ZebTec system (Tecniplast; Buguggiate, Italy). Embryos were kept in standard embryo medium (E3) at 28.5 °C for normal development. To obtain embryos at 36 h post fertilization (hpf), eggs were incubated for 24 h at 28.5 °C and for another 24 h at 24 °C. Embryos were manually dechorionated with forceps after 24 hpf. To prevent pigmentation, embryos were treated with 0.3 % propylthiouracil (PTU) starting at approximately 24 hpf.

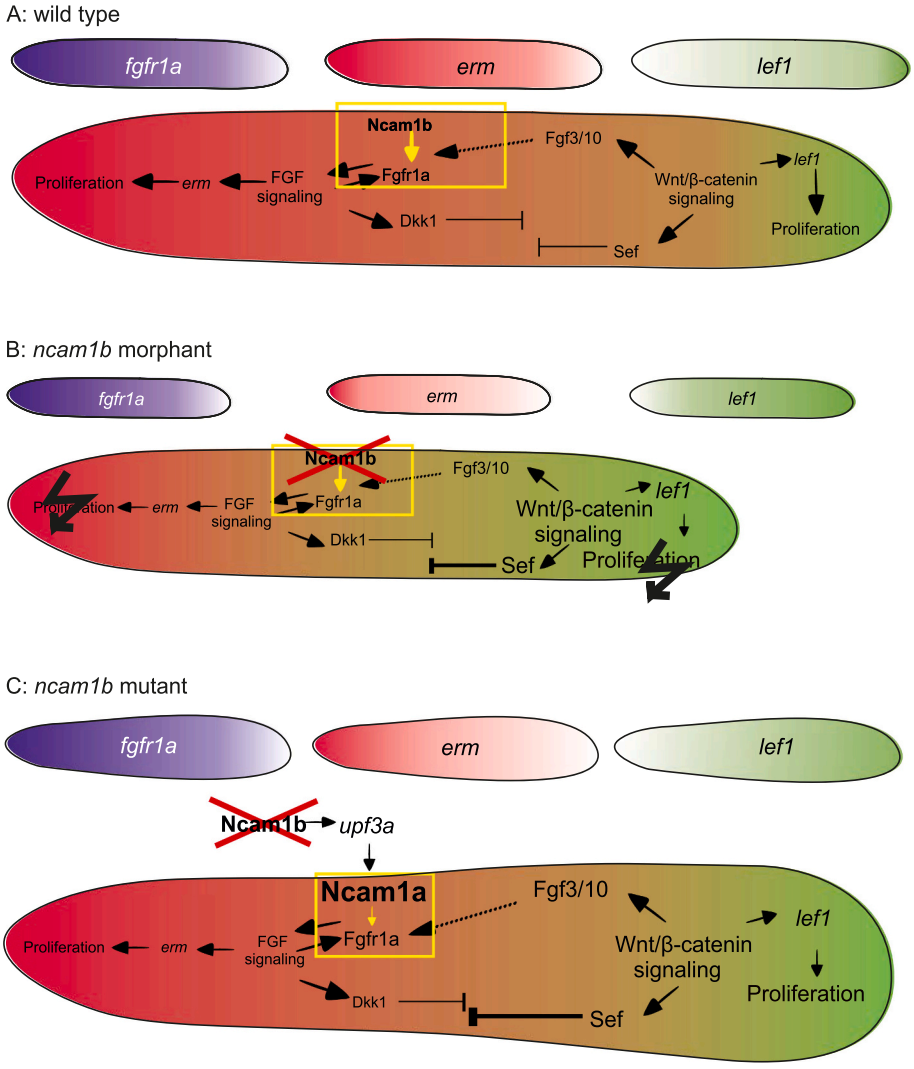

Fig. 6. Model of signaling in the migrating primordium in WT, *ncam1b* morphant, and *ncam1b* mutant. Rostral is left, caudal is right. Small primordia depict *fgfr1a* (purple), *erm* (red), and *lef1* (green) expression distributions, respectively. The large primordia represent overall complex signaling. *erm* (red) and *lef1* (green) expression regions are color-coded. The yellow box highlights the interaction of Ncam1b or Ncam1a with Fgfr1a. Black flashes indicate severely disrupted proliferation.

Staging refers to Kimmel et al. (1995).

4.2. Morpholino injection

Morpholino components were pressure-injected into the yolk at the 1-cell stage. Morpholinos (Gene Tools, Oregon, USA) were used in the following concentrations per embryo: *ncam1b*ATG MO (5'-AGATTATCGCCTTGGTCGGAAACAT-3'), 4 ng (Dries et al., 2021); *ncam1a*5'UTR MO (5'-TTCCGTGTAGAATAGGTAGAGTTGG-3'), 4 ng (Dries et al., 2021); *upf3a*-ATG MO (5'-TCTGCTCCTTTTCAGACCTCATATC-3'), 4 ng (Xie et al., 2023).

4.3. Germ line mutagenesis

Two distinct *ncam1b* mutants were generated using CRISPR/Cas9 genome editing: the *ncam1b* Premature Stop Codon (*n1b* -/- PMSC) mutant and the *ncam1b* deletion (*n1b* -/- Del) mutant. For both mutants, crRNA, tracrRNA (hereafter referred to as guide RNA or gRNA when combined) and Cas9 protein (all from Integrated DNA Technologies (IDT); Coralville, Iowa, USA) were applied according to the IDT protocol *via* injection into one-cell stage embryos. crRNA targeting *ncam1b* were designed using the CRISPOR web tool.

The zebrafish mutant line *ncam1b*^{ka901} (*n1b* -/- PMSC) was created using a single gRNA targeting exon 1 near the *ncam1b* start codon, binding downstream of it. This resulted in a one-base deletion causing a frameshift and premature stop codon. Specifically, the following sequence alterations were introduced on chromosome 15: position 18,369,041A > G, position 18,369,042A > G, and an insertion of G at position 18,369,044. For the zebrafish mutant line *ncam1b*^{ka902} (*n1b* -/- Del), two gRNAs were co-injected: one targeting the same sequence in exon 1 as the *n1b* -/- PMSC mutant, and another targeting a sequence downstream of the stop codon. This method resulted in a 205,908-base pair deletion, eliminating nearly the entire *ncam1b* gene, including both exons and introns. Specifically, the deletion spans chromosome 15 from position 18,369,037 to 18,575,755.

For both mutants, injected fish were grown to adulthood and outcrossed to identify those transmitting the mutations. Homozygous mutant parents were crossed to obtain mutant embryos for further studies.

4.4. Genotyping

Genotyping was performed using genomic DNA from individual or pooled embryos. For adult fish, DNA was extracted *via* skin swabbing following (Tilley et al., 2020). DNA isolation was performed using the Hot Shot method from Meeker et al., (2007). The *n1b* -/- PMSC mutants were identified by PCR, followed by sequencing to confirm the one-base deletion (Supp. 1 B).

For *n1b* -/- Del mutants, PCR was performed using primers 1f (5'GGCTTTGGTTCAGTGCTTCA-3') and 1r (5'-GCCCAGTCAATCGTTCAGTC-3') (Supp. 1 A).

In wild-type DNA, the ~ 200,000 bp distance between primers prevented amplification, while in mutant alleles, the deletion reduced this distance to ~ 700 bp, allowing successful amplification (Supp. 1 A'). Sequencing confirmed the deletion (Supp. 1 A''). For accurate genotyping of progeny from heterozygous carriers, a second PCR was conducted using primers 2f (5'CCTCTTTCTCGGTCAGATGG-3') and 2r (5'-CCAGTGACACCAGCATCACC-3'), with 2r annealing between the two target regions (Supp. 1 A'). This strategy enables to distinguish between WT and mutated alleles.

4.5. Immunostaining of zebrafish larvae

Immunostaining was performed following zebrafish standard procedures as previously described (Marx et al., 2007). Ncam1a and Ncam1b were detected by rabbit anti-NCAM and anti-PCAM kindly provided by Yoshihiro Yoshihara (RIKEN Center for Brain Science, Japan) (both 1:1000). After fluorescence *in situ* hybridization, GFP intensity in *Tg(ClaudinB::lynGFP)* embryos was enhanced by using chicken anti-GFP (1:1000; abcam; Cambridge, GB).

Embryos were subsequently placed in secondary antibody for 2 h at room temperature. For secondary antibody staining, Alexa488 (1:1000; abcam; Cambridge, GB) and cy3 (1:1000; Dianova; Hamburg, Germany) were used as chromophores. Mounting was performed in 20 % Mowiol.

4.6. Whole-mount fluorescence in situ hybridization

Whole-mount fluorescence *in situ* hybridization (FISH) was conducted using a protocol following (Lauter et al., 2014). Digoxigenin- and fluorescein-labeled probes were synthesized from plasmid DNA, with 200 ng of each probe being used for hybridization. Plasmids for *erm* (Scholpp et al., 2004) and *lef1* were generously provided by Steffen Scholpp (University of Exeter, UK). The *fgfr1a* probe was cloned from zebrafish cDNA (Dries et al., 2021). For fluorescent staining, TSA Cyanine 3 (produced in-house — special thanks to Dr. Franco Weth for preparation) and TSA-Plus Cyanine 5 (Perkin Elmer; Shelton, United States) were used. Following hybridization, embryos were immunostained with chicken anti-GFP (1:1000; Abcam, Cambridge, UK) and mounted in 20 % Mowiol.

4.7. BrdU assay

Cellular proliferation was analyzed using bromodeoxyuridine (BrdU; Sigma-Aldrich; Missouri, USA), containing 15 % DMSO. The BrdU incorporation protocol was adapted from Dries et al. (2021), with minor modifications. Embryos were incubated with BrdU for 20 min on ice, followed by 20 min at 28.5 °C, and subsequently fixed. DNA denaturation was performed using 2 N HCl for 15 min at 37 °C. Immunostaining was carried out with primary antibodies anti-BrdU (mouse, 1:100; Abcam, Cambridge, UK) and anti-GFP (chicken, 1:1000; Abcam, Cambridge, UK). The secondary antibody used was Alexa Fluor 488 (1:1000; Molecular Probes, Oregon, USA) and DAPI (1:1000; Carl Roth, Karlsruhe, Germany). Zone determination in the primordium relied on cell morphology. Cells in the Leading Zone display random orientation, while those in the Trailing Zone organize into rosette-like proneuromasts (Fig. 2 J).

4.8. Droplet digital PCR

An Automated Droplet Generator (Bio-Rad, Hercules, USA) was used to generate up to 20,000 reactions for ddPCR. The digital analysis of the individual droplets was performed using the QX200 Droplet Reader and the associated QuantaSoft software (Version 1.7.4, Bio-Rad). Gene expression was normalized relative to β-actin, and then the expression was normalized to wild type. All reactions were performed in technical duplicates; the results are the mean value of biological triplicates or quadruplicate. Primers: β-actin: forward: (5'- CGAGCAGGAGATGGGAACC-3') and reverse (5'-CAACGGAAACGCTCATTGC-3'); *ncam1a*: forward: (5'-GCACCGACCCTAAACCTACT-3') and reverse (5'GGAATTCTTGGCAGGGTCAC-3'); *ncam1b*: forward: (5'-CGCCATTATCGTGTGTGATGT-3') and reverse (5'-CCACGGGCTTTAATACGACC-3').

4.9. Sequence analysis

The DNA sequencing was performed by Eurofins Genomics (Ebersberg, Germany) using Sanger sequencing. For sequence analysis and alignment, we used the free version of CLC Sequence Viewer (Qiagen Bioinformatics).

4.10. Quantification and statistical analysis

For measurements of primordia size and migration distance, we utilized Fiji by ImageJ. Only *Tg(ClaudinB::EGFP)* positive embryos, identified by their EGFP signal, were imaged and analyzed for the quantification of phenotypes in Fig. 1. The FISH samples were imaged using ZEISS Axio Imager.Z1 for quantification. Images were processed and analyzed using the ZEN 2 lite software (Zeiss) and the open-source Fiji distribution of ImageJ. Since not all embryos in Fig. 2 A–F were *Tg (ClaudinB::EGFP)* positive, the total area of the primordium was determined by overlaying the signals from the *fgfr1a/lef1* or *erm/lef1* channels. The resulting area was used as the total area of the primordium. Representative pictures in all figures were imaged using LSM800 from Zeiss. For the quantification of Ncam1a expression in primI, wild type and *ncam1b* mutant embryos were processed in parallel under identical conditions for each experiment. Mean grey value was measured within the defined region of the primordium using Fiji, and mutant mean grey values were normalized to wild type mean grey values for comparison. This standardized workflow ensured consistency across all embryos and minimized variability in staining and analysis, providing reliable and reproducible results. Statistical analysis was performed using Excel and Origin 2019. For significance calculations, we utilized either the *t*-test, Chi-squared (χ^2) analysis or ANOVA analysis. When relative values were compared a two-tailed one-sample *t*-test was applied. For comparisons of original data between two independent groups, a two-tailed two-sample *t*-test was used. Categorical data were analyzed using the Chi-squared (χ^2) test. Group differences were assessed using a one-way ANOVA, followed by Scheffé post hoc comparisons. All tests were conducted at a significance level of $\alpha = 0.05$. All diagrams were created using Origin 2019. Bar charts display the mean of the medians from individual experiments, with the whiskers representing the standard error.

CRediT authorship contribution statement

Annemarie Lange: Writing – original draft, Visualization, Validation, Project administration, Methodology, Investigation, Formal analysis, Data curation, Conceptualization. **Martin Bastmeyer:** Writing – review & editing, Supervision, Resources, Funding acquisition, Conceptualization. **Joachim Bentrop:** Writing – review & editing, Writing – original draft, Supervision, Conceptualization.

Declaration of Competing Interest

The authors declare that they have no known competing financial interests or personal relationships that could have appeared to influence the work reported in this paper.

Acknowledgement

We thank Dr. Steffen Scholpp for providing *lef1* and *erm in situ* probes, Dr. Darren Gilmour for the *Tg(ClaudinB::lynGFP)* zebrafish line, and Dr. Yoshihiro Yoshihara for Ncam1a and Ncam1b antibodies. We thank Dr. Holger Puchta's lab for providing access to the ddPCR equipment. We are thankful for Kerstin Weber's excellent technical assistance.

Appendix A. Supporting information

Supplementary data associated with this article can be found in the online version at doi:10.1016/j.ejcb.2025.151500.

Data availability

Data will be made available on request.

References

Aman, A., Piotrowski, T., 2008. Wnt/β-catenin and Fgf signaling control collective cell migration by restricting chemokine receptor expression. Dev. Cell 15 (5), 749–761. https://doi.org/10.1016/J.DEVCEL.2008.10.002.

Cunningham, B.A., Hemperly, J.J., Murray, B.A., Prediger, E.A., Brackenbury, R., Edelman, G.M., 1987. Neural cell adhesion molecule: structure, immunoglobulin-like domains, cell surface modulation, and alternative RNA splicing. Science 236 (4803), 799–806. https://doi.org/10.1126/SCIENCE.3576199.

Dambly-Chaudière, C., Cubedo, N., Ghysen, A., 2007. Control of cell migration in the development of the posterior lateral line: antagonistic interactions between the chemokine receptors CXCR4 and CXCR7/RDC1. BMC Dev. Biol. 7. https://doi.org/10.1186/1471-213X-7-23.

Dries, R., Lange, A., Heiny, S., Berghaus, K.I., Bastmeyer, M., Bentrop, J., 2021. Cell proliferation and collective cell migration during zebrafish lateral line system development are regulated by Ncam/Fgf-receptor interactions. Front. Cell Dev. Biol. 8. https://doi.org/10.3389/FCELL.2020.591011.

Dykgraaf, S., 1933. Untersuchungen über die Funktion der Seitenorgane an Fischen. Z. für Vgl. Physiol. 20 (1–2), 162–214. https://doi.org/10.1007/BF00340757/METRICS.

El-Brolosy, M.A., Kontarakis, Z., Rossi, A., Kuenne, C., Günther, S., Fukuda, N., Kikhi, K., Boezio, G.L.M., Takacs, C.M., Lai, S.-L., Fukuda, R., Gerri, C., Giraldez, A.J., Stainier, D.Y.R., 2019. Genetic compensation triggered by mutant mRNA degradation. Nature 568 (7751), 193–197. https://doi.org/10.1038/s41586-019-1064-z.

Gamba, L., Cubedo, N., Lutfalla, G., Ghysen, A., Dambly-Chaudiere, C., 2010. Lef1 controls patterning and proliferation in the posterior lateral line system of zebrafish. Dev. Dyn. 239, 3163–3171. https://doi.org/10.1002/dvdy.22469.

Ghysen, A., Dambly-Chaudière, C., 2007. The lateral line microcosmos. Genes Dev. 21 (17), 2118–2130. https://doi.org/10.1101/GAD.1568407.

Gilmour, D.T., Maischein, H.M., Nüsslein-Volhard, C., 2002. Migration and function of a glial subtype in the vertebrate peripheral nervous system. Neuron 34 (4), 577–588. https://doi.org/10.1016/S0896-6273(02)00683-9.

Haas, P., Gilmour, D., 2006. Chemokine signaling mediates self-organizing tissue migration in the zebrafish lateral line. Dev. Cell 10 (5), 673–680. https://doi.org/10.1016/J.DEVCEL.2006.02.019.

Hinsby, A.M., Lundfald, L., Ditlevsen, D.K., Korshunova, I., Juhl, L., Meakin, S.O., Berezin, V., Bock, E., 2004. ShcA regulates neurite outgrowth stimulated by neural cell adhesion molecule but not by fibroblast growth factor 2: evidence for a distinct fibroblast growth factor receptor response to neural cell adhesion molecule activation. J. Neurochem. 91 (3), 694–703. https://doi.org/10.1111/J.1471-4159.2004.02772.X.

Kettleborough, R.N.W., Busch-Nentwich, E.M., Harvey, S.A., Dooley, C.M., Bruijn, E.D., Eeden, F.V., Sealy, I., White, R.J., Herd, C., Nijman, I.J., Fényes, F., Mehroke, S., Scahill, C., Gibbons, R., Wali, N., Carruthers, S., Hall, A., Yen, J., Cuppen, E., Stemple, D.L., 2013. A systematic genome-wide analysis of zebrafish protein-coding gene function. Nature 496 (7446), 494–497. https://doi.org/10.1038/NATURE11992.

Kimmel, C.B., Ballard, W.W., Kimmel, S.R., Ullmann, B., Schilling, T.F., 1995. Stages of embryonic development of the zebrafish. Dev. Dyn. Off. Publ. Am. Assoc. Anat. 203 (3), 253–310. https://doi.org/10.1002/AJA.1002030302.

Kok, F.O., Shin, M., Ni, C.W., Gupta, A., Grosse, A.S., vanImpel, A., Kirchmaier, B.C., Peterson-Maduro, J., Kourkoulis, G., Male, I., DeSantis, D.F., Sheppard-Tindell, S., Ebarasi, L., Betsholtz, C., Schulte-Merker, S., Wolfe, S.A., Lawson, N.D., 2015. Reverse genetic screening reveals poor correlation between morpholino-induced and mutant phenotypes in zebrafish. Dev. Cell 32 (1), 97–108. https://doi.org/10.1016/J.DEVCEL.2014.11.018.

Langhauser, M., Ustinova, J., Rivera-Milla, E., Ivannikov, D., Seidl, C., Slomka, C., Finne, J., Yoshihara, Y., Bastmeyer, M., Bentrop, J., 2012. Ncam1a and Ncam1b: two carriers of polysialic acid with different functions in the developing zebrafish nervous system. Glycobiology 22 (2), 196–209. https://doi.org/10.1093/GLYCOB/CWR129.

Lauter, G., Söll, I., Hauptmann, G., 2014. Sensitive whole-mount fluorescent in situ hybridization in zebrafish using enhanced tyramide signal amplification. In: Sprecher (Hrsg.), S.G. (Ed.), Brain Development, Bd. 1082. Humana Press, pp. S.175–S.185. https://doi.org/10.1007/978-1-62703-655-9_12.

Lecaudey, V., Cakan-Akdogan, G., Norton, W.H.J., Gilmour, D., 2008. Dynamic Fgf signaling couples morphogenesis and migration in the zebrafish lateral line primordium. Development 135 (16), 2695–2705. https://doi.org/10.1242/DEV.025981.

Lush, M.E., Piotrowski, T., 2014. Sensory hair cell regeneration in the zebrafish lateral line. Dev. Dyn. 243 (10), 1187–1202. https://doi.org/10.1002/DVDY.24167.

Lykke-Andersen, S., Jensen, T.H., 2015. Nonsense-mediated mRNA decay: an intricate machinery that shapes transcriptomes. Nat. Rev. Mol. Cell Biol. 16 (11), 665–677. https://doi.org/10.1038/nrm4063.

Ma, Z., Zhu, P., Shi, H., Guo, L., Zhang, Q., Chen, Y., Chen, S., Zhang, Z., Peng, J., Chen, J., 2019. PTC-bearing mRNA elicits a genetic compensation response via Upf3a and COMPASS components. Nature 568 (7751), 259–263. https://doi.org/10.1038/s41586-019-1057-y.

Marx, M., Rivera-Milla, E., Stummeyer, K., Gerardy-Schahn, R., Bastmeyer, M., 2007. Divergent evolution of the vertebrate polysialyltransferase *Stx* and *Pst* genes revealed by fish-to-mammal comparison. Dev. Biol. 306 (2), 560–571. https://doi.org/10.1016/j.ydbio.2007.03.032.

McGraw, H.F., Drerup, C.M., Culbertson, M.D., Linbo, T., Raible, D.W., Nechiporuk, A.V., 2011. Lef1 is required for progenitor cell identity in the zebrafish lateral line

primordium. Development 138 (18), 3921–3930. https://doi.org/10.1242/DEV.062554.
Meeker, N.D., Hutchinson, S.A., Ho, L., Trede, N.S., 2007. Method for Isolation of PCR-Ready Genomic DNA from Zebrafish Tissues. ⟨https://www.tandfonline.com/doi/epdf/10.2144/000112619?needAccess=true⟩.
Metcalfe, W.K., Kimmel, C.B., Schabtach, E., 1985. Anatomy of the posterior lateral line system in young larvae of the zebrafish. J. Comp. Neurol. 233 (3), 377–389. https://doi.org/10.1002/CNE.902330307.
Mizuno, T., Kawasaki, M., Nakahira, M., Kagamiyama, H., Kikuchi, Y., Okamoto, H., Mori, K., Yoshihara, Y., 2001. Molecular diversity in zebrafish NCAM family: three members with different VASE usage and distinct localization. Mol. Cell. Neurosci. 18 (1), 119–130. https://doi.org/10.1006/MCNE.2001.1007.
Rossi, A., Kontarakis, Z., Gerri, C., Nolte, H., Hölper, S., Krüger, M., Stainier, D.Y.R., 2015. Genetic compensation induced by deleterious mutations but not gene knockdowns. Nature 524 (7564), 230–233. https://doi.org/10.1038/NATURE14580.
Scholpp, S., Groth, C., Lohs, C., Lardelli, M., Brand, M., 2004. Zebrafish fgfr1 is a member of the fgf8 synexpression group and is required for fgf8 signalling at the midbrain-hindbrain boundary. Dev. Genes Evol. 214 (6), 285–295. https://doi.org/10.1007/s00427-004-0409-1.
Shum, E.Y., Jones, S.H., Shao, A., Chousal, J.N., Krause, M.D., Chan, W.-K., Lou, C.-H., Espinoza, J.L., Song, H.-W., Phan, M.H., Ramaiah, M., Huang, L., McCarrey, J.R., Peterson, K.J., De Rooij, D.G., Cook-Andersen, H., Wilkinson, M.F., 2016. The antagonistic gene paralogs *Upf3a* and *Upf3b* govern nonsense-mediated RNA decay. Cell 165 (2), 382–395. https://doi.org/10.1016/j.cell.2016.02.046.
Tilley, C.A., Gutierrez, H.C., Sebire, M., Obasaju, O., Reichmann, F., Katsiadaki, I., Barber, I., Norton, W.H., 2020. Skin swabbing is a refined technique to collect DNA from model fish species. Sci. Rep. 10 (1), 1–17.
Vandepoele, K., Vos, W.D., Taylor, J.S., Meyer, A., Peer, Y.V.D., 2004. Major events in the genome evolution of vertebrates: paranome age and size differ considerably between ray-finned fishes and land vertebrates. Proc. Natl. Acad. Sci. USA 101 (6), 1638–1643. https://doi.org/10.1073/PNAS.0307968100.
Xie, A., Ma, Z., Wang, J., Zhang, Y., Chen, Y., Yang, C., Chen, J., Peng, J., 2023. Upf3a but not Upf1 mediates the genetic compensation response induced by leg1 deleterious mutations in an H3K4me3-independent manner. Cell Discov. 9 (1), 1–16. https://doi.org/10.1038/s41421-023-00550-2.
Yi, Z., Arvola, R.M., Myers, S., Dilsavor, C.N., Abu Alhasan, R., Carter, B.N., Patton, R.D., Bundschuh, R., Singh, G., 2022. Mammalian UPF3A and UPF3B can activate nonsense-mediated mRNA decay independently of their exon junction complex binding. EMBO J. 41 (10), e109202. https://doi.org/10.15252/embj.2021109202.
Zhu, P., Ma, Z., Guo, L., Zhang, W., Zhang, Q., Zhao, T., Jiang, K., Peng, J., Chen, J., 2017. Short body length phenotype is compensated by the upregulation of nidogen family members in a deleterious nid1a mutation of zebrafish. J. Genet. Genom. = Yi chuan xue bao 44 (11), 553–556. https://doi.org/10.1016/J.JGG.2017.09.011.